



Cohesional behaviours in pyroclastic material and the implications for deposit architecture

Nemi Walding^{1,2} · Rebecca Williams² · Pete Rowley³ · Natasha Dowey⁴

Received: 20 June 2023 / Accepted: 11 October 2023 / Published online: 27 October 2023
© The Author(s) 2023

Abstract

Pyroclastic density currents (PDCs) are hazardous, multiphase currents of heterogeneous volcanic material and gas. Moisture (as liquid or gas) can enter a PDC through external (e.g., interaction with bodies of water) or internal (e.g., initial eruptive activity style) processes, and the presence of moisture can be recorded within distinct deposit layers. We use analogue experiments to explore the behaviour of pyroclastic material with increasing addition of moisture from 0.00–10.00% wt. Our results show that (1) the cohesivity of pyroclastic material changes with the addition of small amounts of moisture, (2) small increases in moisture content change the material properties from a free-flowing material to a non-flowable material, (3) changes in moisture can affect the formation of gas escape structures and fluidisation profiles in pyroclastic material, (4) gas flow through a deposit can lead to a moisture profile and resulting mechanical heterogeneity within the deposit and (5) where gas escape structure growth is hindered by cohesivity driven by moisture, pressure can increase and release in an explosive fashion. This work highlights how a suite of varied gas escape morphologies can form within pyroclastic deposits resulting from moisture content heterogeneity, explaining variation in gas escape structures as well as providing a potential mechanism for secondary explosions.

Keywords Cohesion · Gas escape · Fluidisation · Secondary explosions · Volcaniclastic · Volcanology

Introduction

Pyroclastic density currents (PDC) are hazardous, rapidly moving and often high-temperature volcanic phenomena. These currents are multiphase mixtures of heterogeneous juvenile material, atmospheric gas, and accessory lithic fragments. The high mobility of PDCs has in part been attributed to the onset of fluidisation (Sparks 1976; 1978; Wilson 1984; Branney and Kokelaar 1992, 2002; Roche 2012; Aravena et al. 2021; Breard et al. 2017; 2023): the upward movement of gas counterbalances the force of gravity and supports the

flow (Sparks 1976; Branney and Kokelaar 2002; Cocco et al. 2014). The ability of the material to flow, or its ‘flowability’, depends upon interparticle forces (Van der Waals, electrostatic or capillary forces). These forces can be influenced by bulk composition and material physical properties such as particle size, density, shape and moisture content (Roche et al. 2004; Rios 2006; Druitt et al. 2007; Leturia et al. 2014).

Fluidisation in PDCs can be initiated from formation and maintained throughout the course of the flow by transport on steep slopes, flow channelisation (Kelfoun and Gueugneau 2022), substrate evaporation (i.e., steam generated from interaction with surfaces with moisture content or bodies of water), bulk self-fluidisation or ambient air entrainment (Sparks 1978; Branney and Kokelaar 2002; Chedeville and Roche 2015; Valentine and Sweeny 2018; Kelfoun and Gueugneau 2022, Breard et al. 2023). Sedimentation fluidisation (or, hindered settling) and particle-self fluidisation is the interstitial gas movement driven by particle settling and compaction (Aravena et al. 2021; Roche 2012; Breard et al. 2017; Chedeville and Roche 2018). On or after deposition, the material will defluidise and particles segregate forming gas escape structures (i.e., fines depleted elutriation pipes) (Wilson 1980; Cas and Wright 1991).

Editorial responsibility: L. Pioli

✉ Nemi Walding
n.walding-2021@hull.ac.uk

¹ Energy and Environment Institute, University of Hull, HU6 7TQ, Hull, UK

² School of Environmental Sciences, University of Hull, Cohen Building, HU6 7RX, Hull, UK

³ University of Bristol, Bristol, UK

⁴ Sheffield Hallam University, Sheffield, UK

Previous analogue investigations into fluidisation behaviours of pyroclastic material and segregation structures have been completed on dry (0% water content; Wilson 1980; 1984) and saturated ($80 \pm 15\%$ water content; Roche et al. 2001) natural pyroclastic material. Experiments completed by Wilson (1980; 1984) used non-cohesive, poorly sorted pyroclastic mixtures and added an influx of gas into the deposit. This resulted in poor fluidisation, along with the creation of gas escape structures dictated by particle size and density. In a study by Roche et al. (2001), aqueous fluidisation within a water-saturated deposit of volcanic material was investigated. These findings revealed that fluid-escape pipes formed easily under conditions of low water flux, leading to localised separation of particle sizes and densities. Combining the results from both experiments, we can conclude that natural pyroclastic material will exhibit aggregative fluidisation, where fluidisation is inhomogeneous throughout the deposit through creation of bubbling and channelling (Branney and Kokelaar 2002; Pacheco-Hoyos et al. 2020). This behaviour arises due to the particle size and density range, regardless of the medium used for fluidisation.

Understanding how moisture, through adsorption of atmospheric humidity, impacts powder material has important industrial applications. Experiments have explored fluidisation behaviours of industrial material with the addition of small volumes of moisture by controlling environment humidity levels. With the introduction of moisture into a material, Van der Waals forces are no longer dominant and liquid bridges connect particles through capillary cohesion; resulting in poor fluidisation behaviours (Wormsbecker and Pugsley 2008; Ludwig et al. 2020; Yehuda and Kalman

2020). A study by Wormsbecker and Pugsley (2008) looked at gas fluidisation behaviours on a semi-saturated (30, 20, 15 and 5 wt.% moisture) powder. Results showed a significant change in fluidisation behaviour associated with the addition of moisture, which were observed in conjunction with the drying states of the material from 30 to 5 wt.%.

Moisture in PDCs and their resulting deposits

Moisture (i.e., water vapour or liquid water) can enter a PDC system during formation at source or as PDCs propagate (Fig. 1). Eruption columns can be water rich due to phreatomagmatic interaction (Self and Sparks 1978; Hurwitz et al. 2003; Houghton et al. 2015; Shimizu et al. 2023) or atmospheric conditions (Vecino et al. 2022). During transport, internal clasts of juvenile magma will exsolve and release water vapour and other volatiles. Experiments have highlighted how magmatic clasts may hold 22–86% vol. residual gas and water content during initiation of PDC transport (Sparks 1978). Gas diffusion times of water content depend on particle size, where larger more porous clasts are thought to release gas more rapidly, and temperature changes, where cooler temperature reduce diffusivity of gas (Sparks 1978).

Moisture may be introduced through a combination of atmospheric (e.g., humidity; Pepin et al. 2017; Camuffo 2019), topographic (e.g., height; Barclay et al. 2006; Duane et al. 2008; Hartmann 2016), climatic (e.g., global location; Barclay et al. 2006) and meteorological (e.g., precipitation) conditions. Furthermore, periods of intense rainfall have been suspected and observed to affect the onset of volcanic

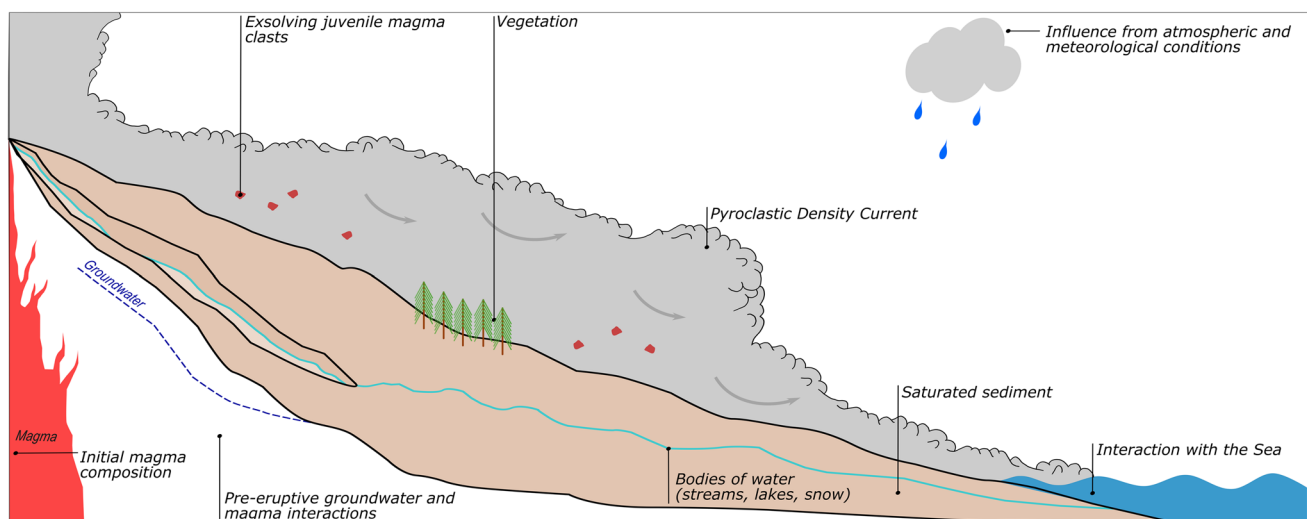


Fig. 1 Schematic illustration of a PDC interacting with sources of moisture across a landscape which have the potential to enter the PDC system and resulting deposits

activity (Barclay et al. 2006; Sahoo et al. 2022 and references therein). Matthews et al. (2009) documented that within 24 h of heavy rainfall, the probability of lava dome collapse at Soufriere Hills Volcano, Montserrat (during the period 1998–2003), increased, resulting in higher moisture availability to the resulting PDCs.

Interaction with external bodies of water (i.e., streams, lakes, sea, snow; Darteville et al. 2002; Cole et al. 1998; 2002), water saturated substrate (Moyer and Swanson 1987; Brown and Branney 2013; Gilbertson et al. 2020) or by the incorporation of vegetation (as observed at Mount Pelé, 1902; Mount St Helens, 1980; Montserrat, 2002; and Fuego Volcano, 2018) can also contribute to moisture within the PDC system. Therefore, we expect moisture content in PDCs and their resultant deposits to be variable in time and space, for example, we can expect high water contents in deposits near bodies of water (i.e., following PDC interaction with a lake) than perhaps in areas where very small amounts of juvenile water are contributing to the overall moisture content (i.e., exsolving juvenile clasts).

The presence of moisture within PDCs can be demonstrated by the presence of peculiar features in their deposit. Moisture has been linked to the formation of wet ash aggregates (e.g., pellets) in pyroclastic deposits (Brown et al. 2010; Van Eaton and Wilson 2013), to elutriation pipes that are rooted in areas of evaporating moisture (i.e., vegetation or water-laden sediments; Pacheco-Hoyos et al. 2020) or by secondary hydroeruptions forming in deposits overlying moisture-rich areas (e.g., Mount St. Helens; Moyer and Swanson 1987). The influence of these relatively small additions of moisture into a PDC system has been largely ignored in analogue and experimental studies, due to the difficulty of using and controlling the characteristics of moisture-affected material. Therefore, prior to experiments, the material is generally dried to remove any residual moisture (Druitt et al. 2004, 2007; Girolami et al. 2008; 2015).

Capillary cohesion

The presence of moisture in a PDC, or in a subsequent deposit, will result in cohesive forces within the interparticulate space. A PDC can reach temperatures > 1000 °C and the resulting deposit can maintain high temperatures for extended periods of time (Dufek 2016; Riehle et al. 1995), and it has been assumed that at these temperatures, the dominant cohesive forces will be electrostatic and Van der Waals forces (Branney and Kokelaar 2002). However, with increasing distance and entrainment, temperatures will decrease (Benage et al. 2016; Dellino et al. 2021; Pensa et al. 2023), and the introduction of moisture will likely lead to the formation of capillary bridges ('capillary condensation'; Ma et al. 2019), resulting in a change of the dominant

interparticulate forces. This is described in Telling et al. (2013), where electrostatic attraction has been observed to be dominant only where water vapour (i.e., humidity) was lower than 71% and in Chigira and Yokoyama (2005), where capillary cohesion became the dominant cohesive force with the addition of moisture into the granular material.

Previous studies have shown that an increase in water content and moisture leads to a drastic change in the physical properties of a given material. For example, in sands, capillary forces were seen to affect the tensile strength of the material until reaching a water-saturated state (Kim and Sture 2008; Chen et al. 2021). Therefore, at lower temperatures it is highly likely that the introduction of moisture into the dynamic (current) and static (deposit) regions will induce variations in material properties. Changes in tensile strength and yield stress may determine how resistant a material is to shear and erode and are important in understanding the flow properties of a material (Pierrat and Caram 1997; LaMarche et al. 2016). Within a PDC deposit, such changes may also influence defluidisation through gas escape.

The experiments detailed herein assess the impact of the addition of small volumes of moisture within natural pyroclastic material. We explore the resulting variations in terms of fluidisation and particle segregation behaviours. Our results provide new and novel insights into the variation of gas escape behaviours and resulting secondary explosions in a defluidising PDC deposit.

Methodology

Source material and sample preparation

Unconsolidated material collected in 2009 from the 2006 Tungurahua, Ecuador, eruptions (provided by U. Küppers, LMU Munich) has been subjected to a range of characterisation tests to elucidate flowability properties and variations with moisture content. The studied material is dark grey/brown and andesitic in chemistry and was sampled from the PDC material deposited during the 2006 VEI 3 eruption (Eychenne et al. 2012). The PDCs, formed from the destabilisation of erupted deposits at the vent (Douillet et al. 2013), reached a maximum of 8.5 km from source and descended 2600–3000 m altitude (Hall et al. 2007; Kelfoun et al. 2009).

Samples were dried in an 80 °C oven for 24 h to ensure the removal of residual and adsorbed moisture, and agglomerations were broken up by sieving prior to addition of water. The experiments were completed using 6 samples of the Tungurahua pyroclastic material (Fig. 2, V1–V6). Samples V1, V4, V5 and V6 were sieved into desired particle size distributions, whereas samples V2 and V3 were kept as sampled at source (ranging from > 74 to 300 μm). For the series of characterisation tests, water was added to the

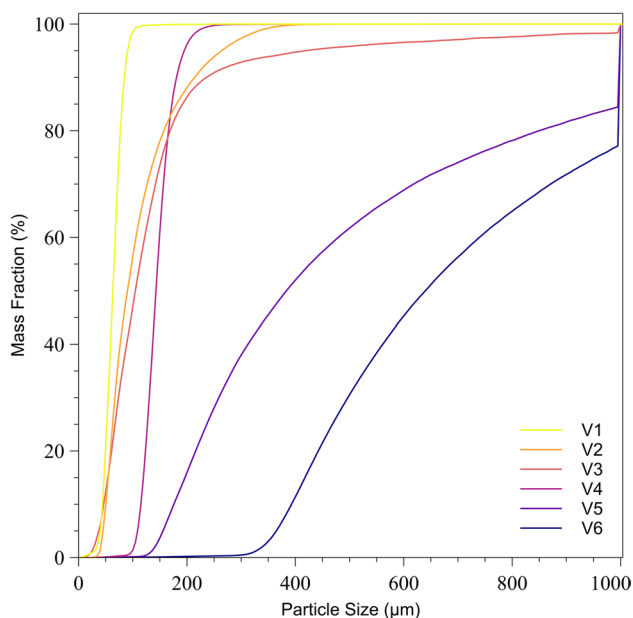


Fig. 2 Particle mass fraction of volcanic material

samples based on weight percentage (0.00, 0.25, 0.50, 1.00, 2.50, 5.00, 7.50, 10.00%). Finally, samples were stirred thoroughly to ensure a homogeneous moisture distribution. All experiments were carried out at room temperature. Whilst the role of temperature may be important in natural material, we were unable to control for this variable in these experiments.

Material characterisation and cohesive behaviour tests

Particle size and shape analysis

Particle analysis of the pyroclastic material was undertaken using a CAMSIZER X2. This uses particle imaging to build particle shape and size characteristics for dry samples. The maximum resolution for particle size and shape of the CAMSIZER is 0.8 µm per pixel. Particles were sieved prior to using the CAMSIZER and samples < 1000 µm were used. Any results from the CAMSIZER erroneously returned as > 1460 µm were removed. The CAMSIZER results allowed us to calculate the sphericity and cumulative size of the samples. The latter were run through GRADISTAT (Blott and Pye 2001) to obtain the particle size mean (\bar{x}), median ($\bar{\phi}$), range (μ), sorting index ((σ)), sorting ((σ_G)), skewness ((Sk)), kurtosis ((K)) and geometric mean (μ). Using methods from Breard et al. (2019), we were then able to calculate the Sauter mean (m) and fines content (%) of the material. All characteristics of each sample are presented in Table 1.

Table 1 Particle size mean (logarithmic), particle size median (log), particle range, fines content (<63 µm), geometric mean, logarithmic (ϕ) method of moments used for mean, sorting, sphericity, skewness and kurtosis, Sauter mean diameter calculated from Breard et al. (2019), Geldart group classification (Geldart 1973) based on mean size of particle

Material	Particle size mean (\bar{x}) ϕ	Particle size median $\bar{\phi}$	Particle size range (μ)	Fines content (%)	Sorting index (σ) ϕ	Sorting (σ_G)	Sphericity	Skewness (Sk) ϕ	Kurtosis (K) ϕ	Sauter mean (m)	Geometric mean (μ)	Geldart group
V1	3.776	3.734	2.5–297.3	35.76	0.428	Well	0.77	1.891	17.00	56.3×10^{-6}	72.93	A
V2	3.215	3.320	15–425	21.41	0.710	Moderate	0.79	-0.524	2.576	21.89×10^{-6}	107.5	A, B
V3	3.118	3.140	5–1000	19.57	0.868	Moderate	0.74	-0.562	4.140	22.9×10^{-6}	115.0	A, B
V4	2.703	2.710	20–650	0.19	0.252	Very well	0.84	0.141	8.536	26.18×10^{-6}	153.5	A, B
V5	1.508	1.568	10–1000	0.11	0.758	Moderate	0.80	-0.103	2.480	55.6×10^{-6}	347.3	A, B
V6	0.833	0.812	10–1000	0.05	0.445	Well	0.79	0.589	8.277	112.84×10^{-6}	557.1	A, B

Geldart’s classification of powders

Geldart (1973) classified powders into four distinctive groups (A–D), each defined by their fluidisation behaviours, which are influenced by particle size and density. These behaviours span a spectrum from ‘very poor’ to ‘excellent’. Group A (30–100 μm) and B (100 μm–1 mm) powders exhibit the most favourable behaviours and expand during fluidisation. On the other hand, Group C, comprising the finest particles (< 20 μm), is governed by interparticulate forces. Group D (> 1 mm) demands higher gas velocities for effective fluidisation. Both group C and D present moderate to very poor fluidisation behaviours, often expressing as slugging, channelling and spouting (Leturia et al. 2014). The pyroclastic materials used in these experiments (Fig. 2) have particle size distributions from 2.5 to 1000 μm, and using the particle mean should exhibit fluidisation behaviours typically of Groups A and B in Geldart’s classification.

Bulk and tapped density

The Carr’s index and Hausner ratio are indicative of flowability and interparticulate behaviours (Hausner 1981) and are useful tools in determining a materials ability to fluidise and flow (Table 2). The Carr’s index measures the strength and compressibility of a material (Eq. 3; Moondra et al. 2018). The Hausner ratio determines the packing of the material and how prone the material is to compaction from external forces (Eq. 4, Yu and Hall 1994; Abdullah and Geldart 1999). A material with a low Hausner ratio indicates better flowability. These parameters are calculated from bulk and tapped density measurements.

Bulk and tapped density measurements describe the mass and volume ratio of a powder or granular material, without and with packing, respectively (Amidon et al. 2017). Tapped density experiments reflect the maximum density achievable through packing. The differences observed in bulk and tapped density measurements are influenced by cohesive attributes of particles (Deb et al. 2018) and can be impacted by the shape and size of a material (Amidon et al. 2017).

Table 2 Relationship between Carr’s compressibility index, Hausner ratio, and flowability behaviours. From (Gorle and Chopade (2020))

CI	HR	Flowability
≤ 10	1.00–1.11	Excellent
11–15	1.12–1.18	Good
16–20	1.19–1.25	Fair
21–25	1.26–1.34	Passable
26–31	1.35–1.45	Poor
32–37	1.46–1.59	Very Poor
> 38	> 1.60	Very Very Poor

Given that volcanic ash displays uneven and angular characteristics (see sphericity; Table 1), not all spaces between particles are eliminated. Bulk and tapped density were calculated for dry samples herein to characterise cohesive behaviour prior to the addition of water (method adapted from United States Pharmacopeia 2015).

Bulk density (ρ_b) was obtained by pouring 100 g of the volcanic material into a 250-mL cylinder and levelling when needed. The unsettled volume was measured, and bulk density calculated using Eq. 1. This procedure was completed three times per sample.

The cylinder was tapped at 150 taps/min, with volume measured every minute until levelled. Using the unsettled apparent volume and final tapped volume, the tapped density (ρ_t ; Eq. 2), Carr’s index (CI; Eq. 3) and the Hausner ratio (HR; Eq. 4) were calculated, where m is mass (g), V_o is the unsettled apparent volume (mL) and V_f is the final tapped volume (mL) (Moondra et al. 2018).

$$\rho_b = \frac{m}{V_o} \tag{1}$$

$$\rho_t = \frac{m}{V_f} \tag{2}$$

$$CI = 100 \left(\frac{\rho_t - \rho_b}{\rho_t} \right) \tag{3}$$

$$HR = \frac{\rho_t}{\rho_b} \tag{4}$$

Angle of repose

The angle of repose (AoR) refers to the static friction coefficient and the angle of internal friction and can be investigated through static (funnel) and dynamic (rotating cylinder drum) methods (Beakawi Al-Hashemi & Baghabra Al-Amoudi 2018) to explore cohesive behaviours of a material (Montanari et al. 2017). AoR results can be interpreted in terms of understanding the flowability of a material (Table 3).

Table 3 Flowability based on angle of repose results (Beakawi Al-Hashemi and Baghabra Al-Amoudi 2018)

Flowability	Angle of repose (°)
Very free flowing	< 30
Free flowing	30–38
Fair to passable flow	38–45
Cohesive	45–55
Very cohesive (non-flowing)	> 55

To determine the static angle of repose (SAoR) for each experiment, samples of 100 g of material were released from a funnel held 3.5 cm over a circular platform (A_v diameter = 12 cm). The height of the cone was measured, and the angle of repose calculated using Eq. 5 (Beakawi Al-Hashemi and Baghabra Al-Amoudi 2018), where h is height and D is base diameter (mm). When the material did not release freely from the funnel, the material was lightly agitated. If the height of the cone reached the base of the funnel, then the funnel was incrementally moved vertically to accommodate the growing cone. This was repeated three times for each experiment.

$$\text{SAoR } (^{\circ}) = \tan^{-1}\left(\frac{2h}{D}\right) \quad (5)$$

Dynamic angle of repose (DAoR) was determined by rotating 100 g of material in a clear cylindrical drum at a constant rate (Smith 2020). This was recorded on video and critical angle (the maximum angle prior to collapse) measurements analysed using ImageJ (Schneider et al. 2012). This was repeated three times.

Fluidisation behaviour tests

Experiments to determine the fluidisation behaviours of the pyroclastic material with increasing moisture contents were completed using a rectangular, near-2D fluidisation chamber with a porous base (following Gilbertson et al. 2020). Homogeneous samples of 200 g of pyroclastic material and water were placed into the chamber and carefully levelled. A manometer probe recorded basal pore pressure changes during each experiment. Gas velocity of dry compressed air (cm/s) was increased incrementally until either a stable, channelised bubbling fluidisation state was achieved, or large amounts of winnowing or pressure build-up occurred. To limit the effects of drying from basal air flow, experiments were carried out with gradual increases in gas flow rate (0.050–0.208 cm/s for dry sediments and 0.451–0.764 cm/s for moisture added sediments) over a period of 01:11–23:51 min.

Table 4 Loose and tapped bulk density, the Hausner ratio, Carr index and flowability

Material	Loose bulk density (kg m ⁻³)	Tapped bulk density (kg m ⁻³)	Hausner ratio	Carr index	Flowability
V1	1310	1420	1.08	7.73	Excellent
V2	1320	1550	1.18	15.13	Good
V3	1380	1610	1.17	14.28	Good
V4	1320	1420	1.07	6.59	Excellent
V5	1280	1440	1.12	10.68	Excellent
V6	1180	1370	1.15	13.37	Good

Limitations

To better isolate the effect of moisture on material behaviours, a number of other parameters linked to natural PDCs, and their deposits were either kept the same or constrained. In nature, pyroclastic material is more polydisperse and showcases a wider distribution of size, density, shape, composition and temperature than the material used in this work. The limitations on the particle size in our experiments originate from (1) the size of the fluidisation tank and the maximum gas velocity, which dictate the range of material particle sizes that can be used, and (2) the need for effective control of the influence of moisture addition. For instance, the finer fractions of material, characterised by an increased surface area, are more likely to be affected by moisture-related effects (Huang et al. 2009). The fines content of a material governs fluidisation, and fine material will readily fluidise at a lower minimum fluidisation velocity than a coarser material (e.g., blocks from a block and ash flow) (Gilbertson et al. 2020). The samples used in this study are analogous to natural fine fractions of pyroclastic material, such as the fines content of a lapilli-tuff ignimbrite facies, an ash-dominated ignimbrite facies or a block and ash flow deposit.

Our work provides insight to the role of moisture content on pyroclastic material. In the discussion, we begin to explore how other parameters (e.g., size, shape) may impact the cohesivity and material behaviour where appropriate. A multivariate analysis to quantify the relative control of moisture versus a wide range of other parameters would be an important follow-on study to this work.

Results

Material properties

The bulk and tapped densities were calculated for pyroclastic samples ranging in sizes from 3.8 ϕ (V1) to coarsest 0.8 ϕ (V6). With increasing particle size, bulk and tapped densities generally decrease (Table 4). Material flowability, as determined by the Hausner ratio and Carr index, is good

(V2, V3, V6) and excellent (V1, V4, V5) under the 0% moisture conditions. The change in flowability between V5 and V6 likely reflects the large increase in geometric mean from 347 (V5) to 557 mm (V6) (Table 1). The excellent flowability in V1, V4 and V5 is likely related to the smaller particle range in V1 and V4 and the low fines content in V5.

The static angle of repose (SAoR) increases with increasing moisture across all volcanic samples (V1–6; Fig. 3). For the 0% moisture condition, the SAoR ranges from 21 (V2, V4, V5) to 23° (V1, V3). Interestingly, these results show that under 0% moisture conditions, the SAoR is broadly similar (within 2°) regardless of particle size or sorting (Fig. 4a).

When increasing moisture contents to 5%, the SAoR values increase to approximately double those achieved with 0% moisture, reaching from 42 (V5, V6) to 47° (V4). However, this relationship is not linear with increasing moisture content (Fig. 4a). All materials show a rapid increase in SAoR with moisture to around 25°. But beyond a moisture content of 0.5%, a division is evident between

the fine and coarse mixtures; those with higher Sauter mean diameters (V2, V3 and V4) quickly increase to SAoR values of ~45° at moisture contents of 2.5%, before becoming invariant with additional moisture content. Mixtures with large Sauter mean diameters (V5, V6) mostly show a more gradual increase in SAoR with moisture content. V5, with a Sauter mean diameter of 55.6×10^{-6} m, shows an intermediate behaviour, whilst V6 with a Sauter mean diameter of 112.9×10^{-6} m shows a more *linear* relationship for SAoR with moisture between 0.5 and 5%. However, V1, with a Sauter mean diameter of 56.3×10^{-6} m, shows a rapid increase, similar to V2, V3 and V4. This may be due to the high fines content and sorting index (Table 1).

The sphericity of the samples is shown in Table 1. Samples used are from the same parent material; therefore, we see no large variation in particle shape (0.74–0.84 in sphericity). In general, the finer material is slightly more angular than the coarser material. We conclude that any differences in sphericity have not influenced the results, and small

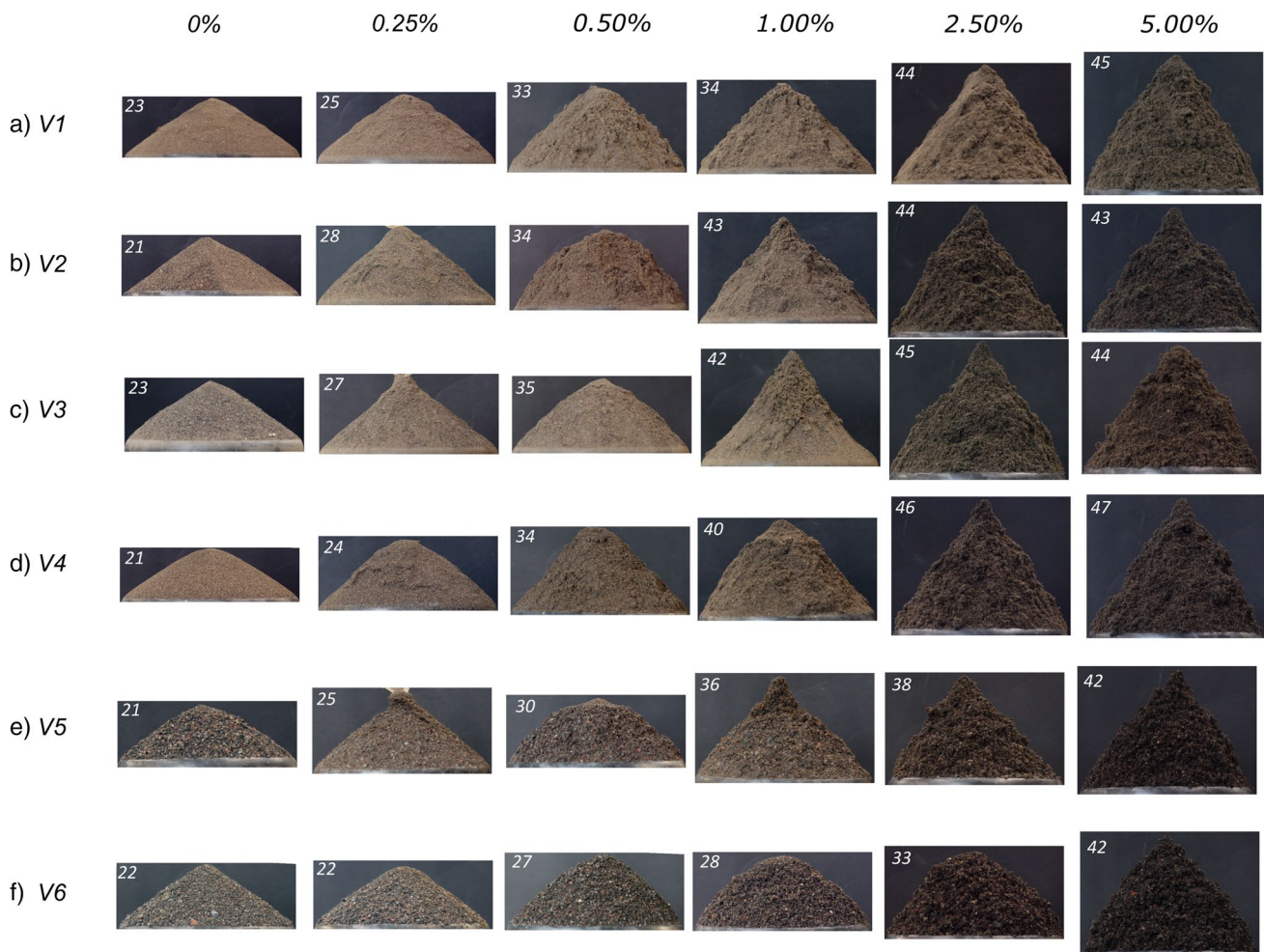


Fig. 3 Representative static angle of repose (SAoR) cone formation of V1–V6. Numbers next to each cone show the average cone height (°)

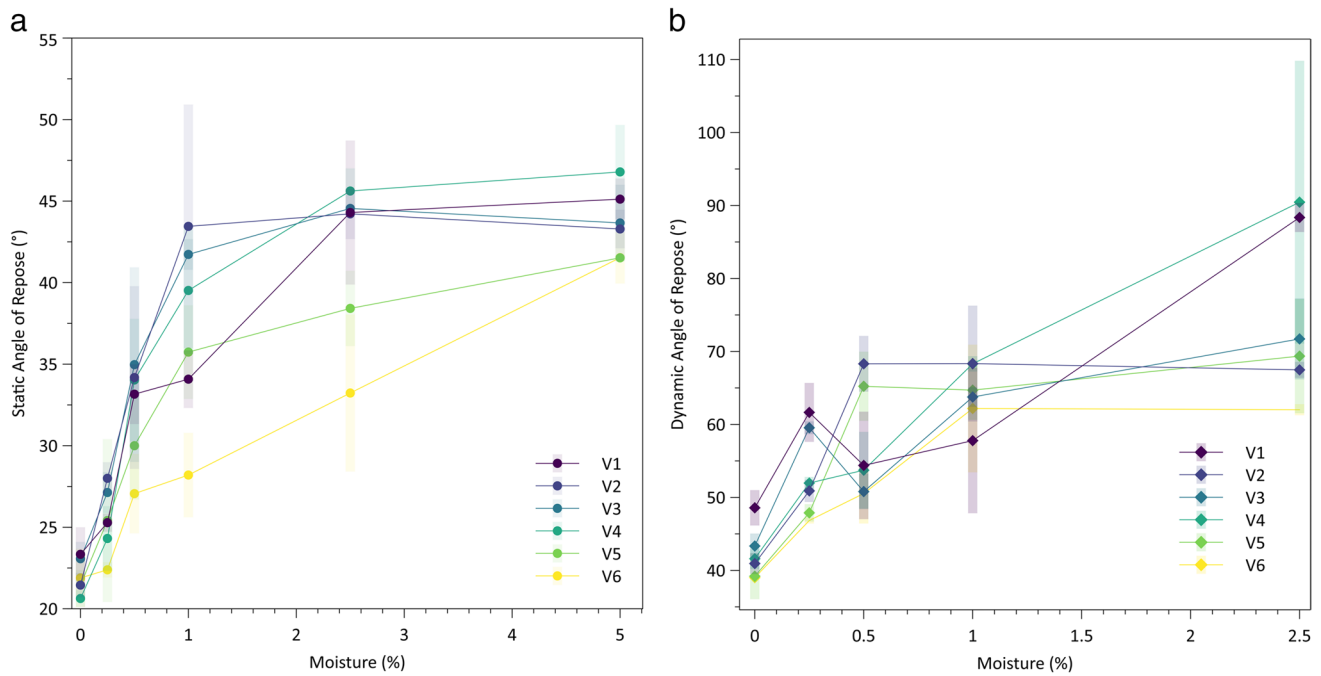


Fig. 4 **a** SAoR for volcanic material with varying moisture percentages with standard deviation error bars; **b** DAoR critical angle of volcanic material with varying moisture percentages with standard deviation error bars

changes in sphericity are not directly related to the cohesive behaviours seen in our experiments.

The results indicate that SAoR is sensitive to increasing values of water in the materials and that relatively small weight percentages can produce very different cohesivities within the mixtures. It is notable that fines-rich mixtures are particularly sensitive to moisture related cohesion, notably at <2% moisture, and this is thought to be due to increased surface area and Sauter mean diameter.

Figure 4 also shows the relationship of dynamic angle of repose experiments (Fig. 4b). Generally, and similar to the SAoR results, there is an increase in the DAoR with increasing moisture. However, in experiments with increasing moisture levels (>2.50%), the material was observed to clump, slide and stick to the outer walls of the drum, complicating the results. Nonetheless, it is important to observe that the Sauter mean relationships detected within the SAoR experiments are not replicated in the DAoR tests.

Fluidisation experiments

Fluidisation behaviours were described via sidewall video analysis of the fluidisation chamber. The observation of gas escape structures (i.e., bubbling, channelling, pocketing, explosive channelling, cracking; Fig. 5a–e) and gas velocity measurements were recorded at varying moisture levels (Fig. 6).

Bubbling gas escape (Fig. 5a) is seen initially in most experiments, where gas bubbles rise from the influx of gas within the deposit. With increasing gas flux, this can lead to channelling, where the material is sorted through vertical channels or via pipe structures forming within the deposit (Fig. 5b). Drying profiles that migrate through the deposit are shown in Fig. 5c. As drying migrates with non-uniformity in the vertical deposit, formation of areas of wet lobes and bubbling dry pockets can be observed, referred to as pocketing (Fig. 5c). Explosive channelling can also be observed in some experiments (Fig. 5d); as the material dries, the upper wet deposit inhibits gas escape and causes a pressure increase and subsequent release (Online Resource 1). Finally, under the highest moisture contents, the material does not form any of the gas escape structures outlined above. Instead, pressure builds until the deposit fractures into cracks where gas can easily permeate through (Fig. 5e; Online Resource 2).

0.00% moisture

At 0.00% moisture for mixtures with moderate sorting (i.e., V2, V3, V5), fine material migrates through gas escape channels (Fig. 5b) in the lower portion of the deposit. The observation of minimum bubbling (U_{mb}) is first seen in the upper fine fraction of the deposit at 0.11 (V2), 0.08 (V3) and 0.42 (V5) cm/s. There is often a separation of fines bubbling in the upper layer, with a mid-area of coarse channelling

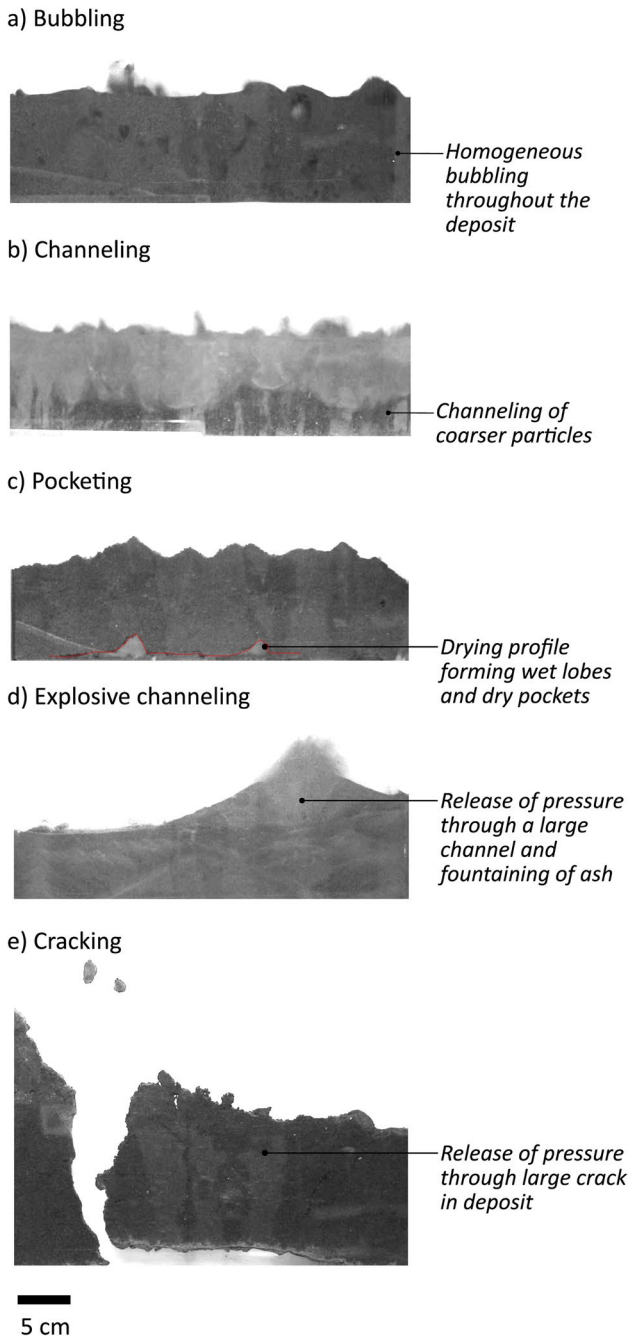


Fig. 5 Examples of the structures recognised across the experiments

(U_{mc}) at 0.13 (V2) and 0.10 (V3) cm/s as fines are being elutriated, and a coarse material layer at the base of the deposit. Bubbling only affects the finer material.

In the mixtures that are well to very well sorted (i.e., V1, V4), bubbles rise uniformly throughout the whole deposit with a U_{mb} of 0.07 (V1) and 0.19 (V4) cm/s. Within the more coarse, well sorted material (V6), bubbles migrate in a sluggish motion from the base of the deposit, with mostly bubbling (U_{mb} 1.60 cm/s) occurring in the upper half of the

deposit and channelling in the lower. This reflects the slight particle size variation of the material used, and therefore, the U_{mb} of the coarser material (Fig. 5b).

0.25% moisture

At 0.25% moisture contents, similar behaviours are observed for V3 (U_{mb} 0.069 cm/s), V5 (U_{mb} 0.22 cm/s) and V6 (U_{mb} 1.25 cm/s) as are observed for 0.00% moisture. For V2 (U_{mb} 0.15 cm/s), V1 (U_{mb} 0.13 cm/s) and V4 (U_{mb} 0.15 cm/s), bubbling begins at the base of the deposit. However, as the surrounding wet deposit begins to dry, this dry material becomes incorporated into the bubbling deposit. In V2, we again see a separation of channelling and bubbling in the lower and upper deposit.

0.50% moisture

At 0.50% moisture, a drying profile can be observed throughout most of the deposit (V4, V5, V6). In the V4 sample, as drying at the base moves throughout the deposit, dry material begins to bubble (U_{mb} 0.28 cm/s), and pressure slowly increases. This is released suddenly (explosive channelling) at 0.54 cm/s through a large channel which cuts through the wet, upper part of the deposit. As the surrounding wet material then begins to dry, it becomes incorporated into the bubbling deposit. In the V5 sample, the drying profile forms lobes of wet material and pockets of dry material. The dry pockets slowly grow until reaching the upper deposit and begin to bubble (U_{mb} 1.04 cm/s). With continued drying as the experiment progresses, similar behaviours to the 0.25% and 0.00% moisture level experiments are observed. After the drying profile has moved through the deposit of V6, similar behaviours to the 0.25% and 0.00% moisture experiments are observed (U_{mb} 1.60 cm/s).

For the V3 material, channels of coarser material begin to slowly move towards the surface. Material begins to dry and is then incorporated into the bubbling deposit (U_{mb} 0.14 cm/s).

1.00% moisture

At 1.00% moisture, V1, V2, and V4 show portions of material at the base of the deposit drying in pockets. The dry material begins to bubble (U_{mb} 0.35, V1; 0.49, V2; 0.42, V4 cm/s) and as the surrounding wet material begins to dry, it is incorporated into the bubbling deposit. In V5 and V6, a distinctive drying profile moves through the deposit. Again, this creates dry pockets of bubbling material (U_{mb} 1.32, V5; 1.81 V6 cm/s) and wet lobes. In V3, pressure slowly builds as gas velocity is increased. Pressure is suddenly released through the formation of an explosive channel (U_{mb} 0.35 cm/s). The

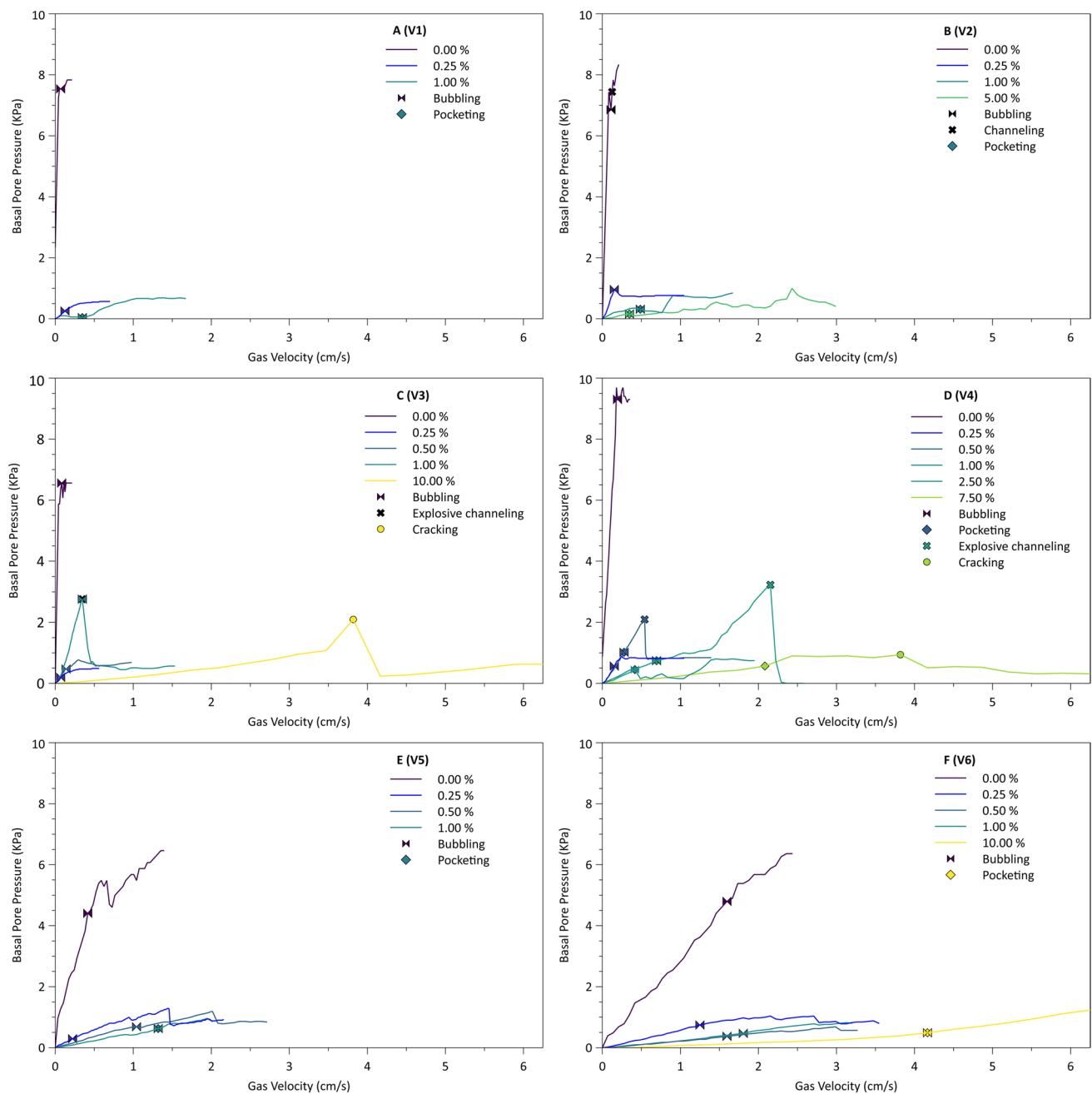


Fig. 6 A–F Fluidisation profiles of V1–V6 with increasing moisture (0.00–10.00%). Symbols show gas escape structure formation

dry deposit then begins to bubble (U_{mb} 0.35 cm/s) and is slowly incorporated into the surrounding drying material.

2.50% moisture

At 2.50%, behaviours of V4 show similar results to 1.00% moisture content: as the base dries, bubbling pockets are formed (U_{mb} 0.70 cm/s) in-between lobes of wet material. In V4, pressure builds until it is suddenly released through an explosive channel (U_{mb} 2.15 cm/s).

5.00% moisture

At 5.00%, V2 shows the deposit drying at the base which forms drying and bubbling (U_{mb} 0.35 cm/s) in pockets, and wet lobes.

7.50% moisture

At 7.50%, a clear drying profile forms through the V4 deposit; cracks begin to form and move through the deposit

until reaching the top and collapsing into pieces (U_{mb} 3.82 cm/s). As gas moved through cracks, there was no dramatic rise and release in pressure.

10.00% moisture

Finally, at 10.00%, V3 forms a clear drying profile within the deposit. Pressure builds before being released suddenly at U_{mb} 3.82 cm/s. This forms a large crack in-between wet material. V6 shows a clear drying profile, as pressure slowly rises as small pockets eventually form and dry material begins to bubble (U_{mb} 4.17 cm/s).

Key observations

The fluidisation experiments clearly demonstrate how small additions of water into pyroclastic material can greatly impact fluidisation behaviours and resulting gas escape structures of a defluidising pyroclastic deposit. Two key observations are apparent in the experiments: (1) the drying profile and (2) pressure build up and release.

The dynamics of the drying profile, as the moisture content is impacted by the fluidising gas, exert a strong control on the distribution of gas escape features, with variations controlled by the grain size of the materials.

As gas flux is increased, a drying profile can move from the base to the top of the deposit. The drying profile forms more easily within the coarser materials (V3–V6). The profile initially rises uniformly across the bed, before becoming irregular as it reaches the top of the deposit. These profiles are noted as they highlight vertical and lateral moisture heterogeneity within the deposit, and their irregular structure determines the formation of drying pockets and wet lobes (Fig. 5c). At low moisture percentages (<2.50%), the drying pocket bubble and the wet lobes begin to dry before being incorporated into the pockets. However, at high moisture contents (>2.50%), moisture-rich lobes remain throughout the experiment, even at high gas velocities. This shows that within a defluidising deposit, a drying profile will lead to lateral and vertical variations in moisture.

In experiments with moisture contents of 0.50–10.00%, explosive channelling (V3, V4) and cracking (V3, V4) can occur. Across the experiments with 0.50–5.00% moisture contents, a wet impermeable cap was observed to form above the drier underlying deposits, with progressive drying of the vertical profile. Pressure builds under the cohesive cap and continues to rise with increasing gas velocity. This eventually results in explosive channelling and a sudden basal pressure drop as the overburden pressure is exceeded. In higher moisture level (5.00–10.00%) experiments, the deposit does not dry as a relatively uniform rising profile. Instead, pressure builds as the gas velocity is increased until

cracks form in the deposit. These cracks act as effective gas escape structures and release the pore pressure.

Discussion

The impact of moisture on pyroclastic material and PDC behaviour is poorly understood, with previous detailed investigations of fluidisation in pyroclastic material having focused on dry (Wilson 1980) and saturated (Roche et al. 2001) end members. However, direct observations have shown that variable amounts of moisture can enter a PDC system (Cole et al. 1998, 2002; Lipman 2019; Vecino et al. 2022), and accretionary lapilli and ash pellets are believed to provide evidence for the presence of moisture within PDCs (Branney and Kokelaar 2002; Brown et al. 2010; Druitt 2014).

Our results show that for the pyroclastic material used within these experiments, (1) the cohesivity of pyroclastic material alters drastically, even with very small concentrations of moisture, (2) moisture addition into pyroclastic material can change flow property behaviours from free flowing to non-flowing, (3) changes in moisture affects fluidisation profiles and gas escape structures, (4) a defluidising deposit can lead to a drying profile, and therefore lateral and vertical heterogeneity within the deposit, and (5) pressure can increase where gas escape is hindered by moisture, which can cause dramatic releases of pressure in an explosive fashion. Here, we discuss the implications of these findings.

Gas escape structures

A variety of gas escape structures were observed in the fluidisation experiments, with many of them related to moisture content. Here, we define three main types of behaviour (Table 5). In type 1 (<0.50% moisture), we see partial fluidisation and segregation of heterogenous material through bubbling and channelling. In a material with a smaller size range, small vertical bubbling occurs across the entirety of

Table 5 Types of behaviour of gas escape observed with increasing moisture in volcanic material

	Type 1	Type 2	Type 3
Moisture range	0.00–0.25%	0.50–5.00%	7.50, 10.00%
Bubbling	Yes	Yes	Yes
Channelling	Yes	Yes	No
Drying profile	No	Yes	Yes
Pocketing	No	Yes	Yes
Explosive channelling	No	Yes	No
Cracking	No	No	Yes

the deposit. During type 2 (0.50–5.0% moisture), an irregular drying profile develops and moves through the deposit from the base. As the drying profile grows, dry pockets of bubbling material begin to form in between irregular lobes of wet material. Explosive channelling also occurs, which releases pressure and facilitates quicker drying of the whole deposit. Finally, during type 3 (7.5–10.0% moisture), similar lobe and pocket structures are formed to type 2 but are accompanied by cracking processes, where fractures in the wet material form to accommodate rapid gas escape. Our experiments represent a defluidising deposit with dry air; in nature, we may expect to see defluidisation of moist air, through contact with bodies of water, for example. Our results demonstrate that moisture addition may hinder or prevent fluidisation and gas escape; therefore, a wet air flux may display strikingly different results. This could not be tested experimentally in this work and would benefit from future investigation.

Roche et al. (2001) investigated the fluidisation behaviour of pyroclastic material where the material was saturated with water (aqueous state) and subjected to an increase in fluid velocity. The findings of Wilson (1980; 1984) and the experiments herein demonstrate gas escape structures forming from an aerated fluidisation state with an increase in gas velocity. In all experiments, aggregative behaviour was observed, and the gas escape structures that formed were consistently depleted in fines and enriched in dense and coarse material. Importantly, Roche et al.'s (2001) research revealed that aqueous gas escape structures (pipes) formed at lower fluid velocities than the aerated structures in Wilson's work (1980) (Fig. 7). This is due to water having a lower terminal velocity than air.

Figure 7 shows that by increasing moisture within a sample, higher gas velocities are required for aggregative fluidisation. Values from Wilson (1980) are based on the first formation of pipes at 0% moisture. Our values are from the first formation of gas escape structures at varying moisture percentages (i.e., bubbling at lower moisture percentages and explosive cracking at the highest). Results from Roche et al. (2001) are based on initial pipe formation at 80% moisture.

Between 10 and 80% moisture, a change in the dominant fluidising medium is inferred, from gas to water. Instead of impeding early fluidisation structures, a large increase in moisture leads to more regular structures forming. This can be explained by changing particle-water states with increasing moisture. Future investigation covering increments between 10 and 80% moisture may be able to define this behaviour change. Aggregative fluidisation mechanisms will result in the segregation of particles through gas escape structures, where fines are winnowed. The nature of segregation will depend on the particle concentration and the size, shape, density and relative proportions of clasts (Sparks 1976; Wilson 1980; 1984; Branney and Kokelaar 2002). We

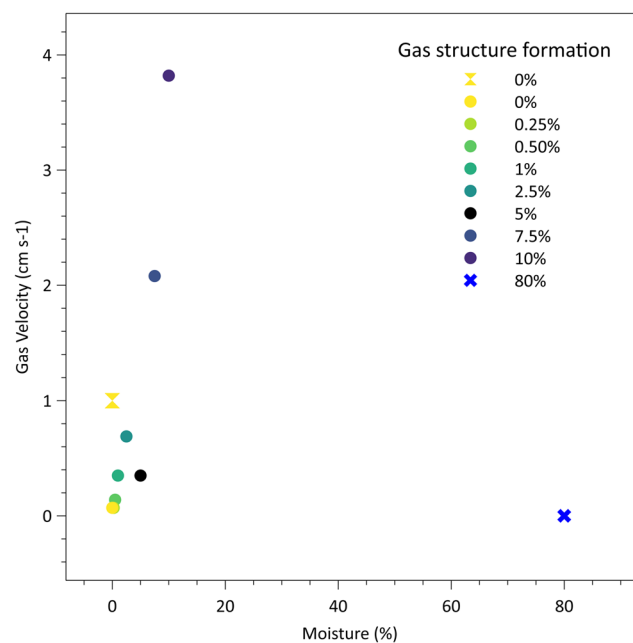


Fig. 7 The gas velocity (cm/s) required to initiate gas escape structures depending on moisture percentage (%). Symbols represent different experimental suites from this study (circles), Wilson (1980) (hourglass) and Roche et al. (2001) (crosses)

find that the moisture content of the deposit also controls this process; segregation structures can change dynamically with drying or become hindered with increasing moisture influence. This is due to our material being in a predominantly capillary state (Kim and Hwang 2003; Kim and Sture 2008). At higher levels of moisture, particles reach a more saturated state, are completely supported by capillary bonds and fluidisation is no longer inhibited (as seen in Roche et al. 2001; Kim and Hwang 2003). We observe that even small moisture influences (as low as 0.50% of weight percentage) into the pyroclastic material used in these experiments may control the formation and nature of gas escape structures.

Application to natural gas escape structures

Our results show that introducing moisture into pyroclastic materials may cause changes in gas escape morphology. Gas escape structures have been recorded and described extensively within field volcanological literature (e.g., Fisher and Schmincke 1984; Cioni et al. 2015; Pacheco-Hoyos et al. 2020). They have been described as pods and pipes displaying single or branching patterns, or as lenticular, curvilinear and crescentic shaped (Wilson 1980; Branney and Kokelaar 2002; Pacheco-Hoyos et al. 2020). They can be spatially arranged within individual layers or can move through multiple layers and are often fines depleted. Our results demonstrate varied morphologies, including vertical channels,

sub-vertical cracks and pods (created by moisture-rich lobes and dry pockets).

Changes in gas escape structures in pyroclastic deposits are thought to be dominated by heterogeneity within the material (e.g., size, density, shape; Wilson 1984; Pacheco-Hoyos et al. 2020). We propose that varying moisture levels will also influence changes in gas escape morphology and may explain circumstances where morphological changes are observed when other conditions appear unchanged. More detailed documentation of morphology of field examples may allow for improved interpretations of depositional environment.

Mechanism for secondary explosions

Secondary explosions in pyroclastic deposits form due to the interaction between water and hot material (Van Westen and Daag 2005). Water in contact with hot pyroclastic material will convert into steam and expand, causing sudden explosive decompression. Secondary explosions form large craters (20–80 m depth) can remobilise large volumes of pyroclastic material and can occur for years after the initial eruption (the 1991 Mount Pinatubo generated secondary explosions for up to a year; Riehle et al. 1995; Van Westen and Daag 2005). Riehle et al. (1995) modelled cooling, degassing and compaction behaviours within thick pyroclastic deposits. High temperatures were most likely to remain elevated within deposits > 50 m thick, with temperatures cooling mostly by groundwater and rainfall. Keating (2005) modelled that the addition of water on a hot deposit can result in increasing pore pressure, in turn exceeding the overburden pressure. This can result in secondary explosions.

Moyer and Swanson (1987) described three styles of secondary explosions—passive degassing (least explosive), ash fountaining and explosive cratering (most explosive)—controlled by thermal energy and the permeability of the overlying material. Analogue experiments investigating the mechanisms of secondary explosions have been performed by Gilbertson et al. (2020). They identified that vertical changes in size fractions, and therefore, a vertical profile of minimum fluidisation velocities, resulted in secondary phreatic explosions. In the experiments of Gilbertson et al. (2020), a deposit capped with coarser material formed an upward doming bed leading to an explosive release of material. This was due to a drag-induced system. The fine-particle layer below acted as a lower minimum fluidisation layer that was unable to fluidise the overlying, coarser layer, resulting in pressure increase and release of gas and particles.

Secondary explosions occur in deposits marked by the occurrence of an active and mobile pore pressure gradient associated with a vertical variation in permeability. Results from our experiments show that increasing moisture levels within the fluidised deposit can lead to impermeable

layers forming through drying at the base of the deposit. By increasing moisture throughout our experiments, we exhibit passive degassing (0%), ash fountaining (> 0.50% wt.) and explosive cratering (> 0.50% wt.) behaviours as described in Moyer and Swanson (1987). After lithostatic pressure of the impermeable wet cap is overcome, explosive channelling (> 0.50% wt.) and cracking (> 7.50% wt.) occurs (the ‘explosive cratering’ of Moyer and Swanson 1987). Similarly, to these works, our results demonstrate the impact of intermediate permeability on secondary explosion styles. We argue that the change from passive degassing to explosive cratering is not only a consequence of thermal energy in the system, but also of internal degassing of a partially fluidised deposit.

Critically, our results suggest a potential new mechanism for secondary explosions that form in a moisture-influenced material (Fig. 8a). In our experiments, the addition of water during deposition results in increased cohesion and tensile strength. As the deposit dries from the base, we see a shift in gas escape as the material begins to dry and bubble. In our model (Fig. 8a), the upper moisture-rich layer inhibits passive degassing and leads to increased pore pressure. With increasing pressure in the deposit, the overburden strength of the wet material is compromised. The result is a sudden pressure release by explosive channelling and cracking, which mimics similar behaviours seen in secondary explosions in pyroclastic deposits.

In a dry deposit later moistened by water (i.e., precipitation), the upper moisture-rich layers of material will create an overall denser material (Fig. 8b). Secondary explosions were observed following the Mt. St. Helens 1980 and Mt. Pinatubo 1991 events (Keating 2005) and were attributed to variations in the permeability of pyroclastic deposits caused by the presence of water (e.g., rainfall and lacustrine environments) (Moyer and Swanson 1987; Manville et al. 2002). It is thought that high pressure towards the base of these pyroclastic deposits (caused by vaporisation of water) led to low-permeable layers preventing the balancing of pore pressures throughout the deposit, which resulted in explosive depressurization (Keating 2005). Keating (2005) suggests that after emplacement, hydrological re-establishment may begin to occur, and interaction with hot overlying pyroclastic material may result in the formation of secondary phreatic explosions.

Our moisture influenced model may provide an explanation for the observations of secondary explosions in deposits that have aggraded with the presence of water (e.g., secondary explosions followed the previous location of the Rogue River; Druitt and Bacon 1986) (Fig. 8a) and that have interacted with rain (e.g., Mt. Pinatubo, Daag and Westen 1996) (Fig. 8b). Rainfall may create a moisture-rich cap to the deposit that is impermeable to degassing from the lower deposit. The increased moisture from the rain would result

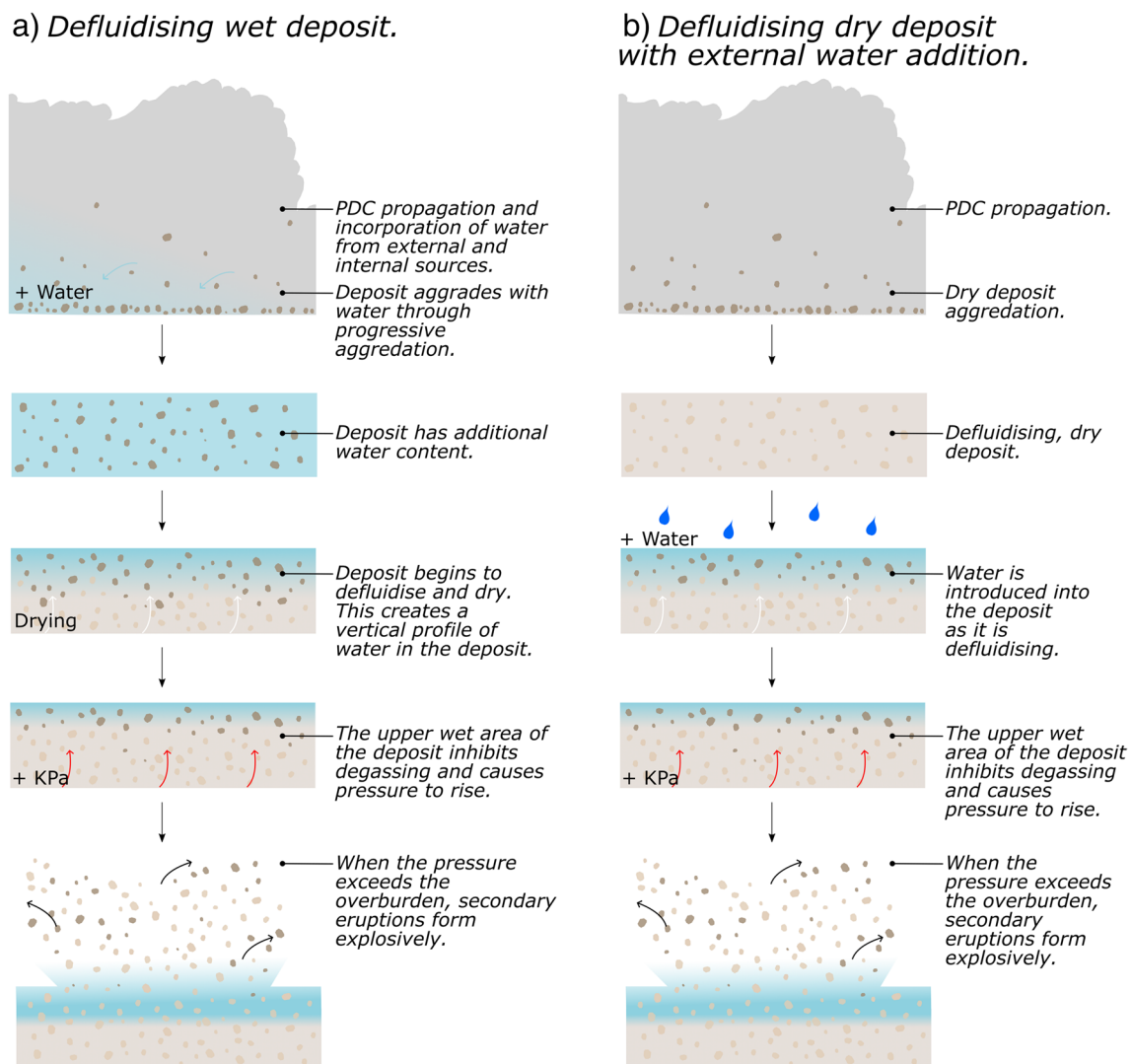


Fig. 8 Moisture-influenced model of secondary explosion formation by **a** a defluidising wet deposit and **b** a defluidising dry deposit with external influences of water

in an increased cohesivity, and therefore, tensile strength, of the material. With gas escape inhibited, pressure may continue to build until the overburden pressure is reached, and degassing is then allowed to escape through a secondary explosion in the deposit.

Implications for deposit remobilisation and preservation

The fine ash fraction of a fines-rich deposit will contribute to increased packing of the material (Lam and Nakagawa 1993; Averardi et al. 2020). In the influence of moisture, where moisture has a greater effect on fines, we would expect the deposit to hold an increased moisture content in the fines portion in comparison to a coarser portion. Within a material with > 30% volume of fines, the stress forces begin to

be dominated by the fine fraction (Li et al. 2020; Breard et al. 2023). A large volume of fines, both with and without moisture, may dramatically alter the deposition and the preservation potential of these layers. Our results show that small amounts of moisture appear to increase the cohesivity of pyroclastic material. A more cohesive deposit may be more resistant to erosion, and remobilisation, meaning that moist layers may be more likely to be preserved in volcanic successions. Additionally, the formation of a drying profile demonstrates both vertical and lateral variation due to an undulating contact between wet and dry material, resulting in vertical and lateral changes in the tensile strength of a deposit. Therefore, erodibility and preservation of layers may be variable. Future work should aim to quantify cohesivity of material directly and determine yield stress and tensile strength. This will enhance our understanding

of material properties and behaviours, allowing us to comprehensively assess their implications for erodibility, remobilisation and preservation.

Implications for PDC flow dynamics

The material behaviours revealed by the BTD, SAoR and DAoR tests raise important questions regarding the impact of moisture within a dynamic, moving PDC. The experiments show that in a dry (0% moisture) state, the material analysed has a low cohesivity as evaluated by the friction angles. As well as fines concentration, sorting is seen to play a key role (Table 1). This can be seen in V1 (5% SAoR: 45°), which is well sorted and displays the largest volumes of fines (35.76%), whereas V4 (5% SAoR: 47°) is very well sorted and has one of the lowest volumes of fine material (0.11%). The excellent flowability seen in V4 may result from its sorting and resulting packing behaviour, which is known to affect flow behaviour (Breard et al. 2023). The DAoR results show contrasting behaviours versus the SAoR results when comparing the Sauter mean diameter. This could suggest that particle size has a greater control on material behaviour in static regimes compared to dynamic regimes. Such an observation has wide ranging implications. For example, Breard et al. (2023) suggests that long run-out distances in block and ash flows (BAFs) were a result of large degrees of fragmentation, with the current becoming more fines rich, and subsequently, the deposit displaying higher packing. These particle size changes result in a dynamically evolving flow, where fines formation and increasing packing behaviour reflect elevated pore pressure within the flow (Breard et al. 2023). Our experiments (V1, V4) show that both fines content and packing can contribute to good flowability behaviours, with implications for the resulting run-out distance of PDCs. Our experiments are limited by particle size distribution and do not contain any blocks so are only modelling the behaviours of the finest fraction. However, it is the fines fraction that controls the fluidisation of PDCs (Gilbertson et al. 2020). The role of large blocks in affecting fluidization and flowability of PDCs is an important avenue for future research (Sparks 1976; Branney and Kokelaar 2002).

The material with the largest volume of fines (V1, V2) is shown to exhibit more cohesive behaviours with increasing moisture (i.e., higher SAoR angle). Sample V4, which is more well sorted, has the highest increase in SAoR values when moisture is added. Our work demonstrates the important role of moisture, even in small amounts, in changing flowability behaviours. We can build a hypothesis that the addition of moisture into a PDC during propagation, with increasing fragmentation of particles and packing during flow, can be a factor in controlling run-out distances—higher moisture contents reduce flowability so may reduce

maximum runout distances, particularly in flows with enhanced fragmentation.

Our results also indicate that the introduction of moisture reduces material fluidization. Expanding on this, future research exploring moisture on fluidised currents would be a valuable extension of the current static fluidisation experiments. This would allow for a better assessment of how moisture influences fluidisation and the resulting behaviours in PDCs.

Conclusion

This work offers insights into the influence of moisture on the behaviour and characteristics of materials deposited from pyroclastic density currents. Our results demonstrate that for certain pyroclastic material, (1) the cohesivity of pyroclastic material changes drastically, even for relatively small additions of moisture (> 0.50%), (2) an increase in moisture can entirely alter flow property behaviour from a free flowing to a non-flowing material, (3) changes in moisture impact fluidisation profiles and gas escape structures, (4) a defluidising deposit can lead to lateral and vertical heterogeneity within the deposit, and (5) pressure can increase where gas escape is hindered by cohesive substrates driven by moisture content, resulting in secondary explosions. Our results build on previous models of secondary explosions in deposits and support the idea that they are formed because of the development of an impermeable capping layer, here created by the addition of moisture. This work further proposes that moisture within a defluidising deposit profile may hinder or change the formation of gas escape structures, which can then lead to pressure increase and release, with implications for the interpretations of the structures within the deposits. Overall, these findings suggest that moisture plays a critical role in PDC flow dynamics and their deposits, with implications for erodibility, preservation potential and our broader understanding of deposit architecture.

Supplementary Information The online version contains supplementary material available at <https://doi.org/10.1007/s00445-023-01682-9>.

Acknowledgements N. W. was supported by the EU Horizon 2020 Programme (Project GEOSTICK 712525). We thank Gilbertson et al. (2020) at the University of Bristol for the use of the fluidisation chamber. Ulrich Küppers is thanked for supplying the pyroclastic material used in these experiments.

Open Access This article is licensed under a Creative Commons Attribution 4.0 International License, which permits use, sharing, adaptation, distribution and reproduction in any medium or format, as long as you give appropriate credit to the original author(s) and the source, provide a link to the Creative Commons licence, and indicate if changes were made. The images or other third party material in this article are included in the article's Creative Commons licence, unless indicated

otherwise in a credit line to the material. If material is not included in the article's Creative Commons licence and your intended use is not permitted by statutory regulation or exceeds the permitted use, you will need to obtain permission directly from the copyright holder. To view a copy of this licence, visit <http://creativecommons.org/licenses/by/4.0/>.

References

- Abdullah EC, Geldart D (1999) The use of bulk density measurements as flowability indicators. *Powder Technol* 102(2):151–165. [https://doi.org/10.1016/S0032-5910\(98\)00208-3](https://doi.org/10.1016/S0032-5910(98)00208-3)
- Amidon GE, Meyer PJ, Mudie DM (2017) Particle, powder, and compact characterization. In: *Developing Solid Oral Dosage Forms*, 2nd edn. Academic Press, pp 271–293. <https://doi.org/10.1016/B978-0-12-802447-8.00010-8>
- Aravena A, Chupin L, Dubois T, Roche O (2021) The influence of gas pore pressure in dense granular flows: numerical simulations versus experiments and implications for pyroclastic density currents. *Bull Volcanol* 83:1–20. <https://doi.org/10.1007/s00445-021-01507-7>
- Averardi A, Cola C, Zeltmann SE, Gupta N (2020) Effect of particle size distribution on the packing of powder beds: a critical discussion relevant to additive manufacturing. *Mater Today Commun* 24:100964. <https://doi.org/10.1016/j.mtcomm.2020.100964>. (ISSN 2352-4928)
- Barclay J, Johnstone JE, Matthews AJ (2006) Meteorological monitoring of an active volcano: implications for eruption prediction. *J Volcanol Geoth Res* 150(4):339–358. <https://doi.org/10.1016/j.jvolgeores.2005.07.020>
- Beakawi Al-Hashemi HM, Baghabra Al-Amoudi OS (2018) A review on the angle of repose of granular materials. *Powder Technol* 330:397–417. <https://doi.org/10.1016/j.powtec.2018.02.003>. (ISSN 0032-5910)
- Benage MC, Dufek J, Mothes PA (2016) Quantifying entrainment in pyroclastic density currents from the Tungurahua eruption, Ecuador: integrating field proxies with numerical simulations. *Geophys Res Lett* 43(13):6932–6941. <https://doi.org/10.1002/2016GL069527>
- Blott SJ, Pye K (2001) GRADISTAT: a grain size distribution and statistics package for the analysis of unconsolidated sediments. *Earth Surf Proc Land* 26:1237–1248
- Branney M, Kokelaar P (1992) A reappraisal of ignimbrite emplacement: progressive aggradation and changes from particulate to non-particulate flow during emplacement of high-grade ignimbrite. Springer-Verlag, pp 504–520
- Branney M, Kokelaar P (2002) *Pyroclastic density currents and the sedimentation of ignimbrites*. The Geological Society, London
- Breard E, Dufek J, Lube G (2017) Enhanced mobility in concentrated pyroclastic density currents: an examination of a self-fluidization mechanism. *Geophys Res Lett* 45:654–664. <https://doi.org/10.1002/2017GL075759>
- Breard E, Jones J, Fullard L, Lube G, Davies C, Dufek J (2019) The permeability of volcanic mixtures—implications for pyroclastic currents. *J Geophys Res Solid Earth* 124(2):1343–1360. <https://doi.org/10.1029/2018JB016544>
- Breard E, Dufek J, Charbonnier S, Gueugneau V, Giachetti T, Walsh B (2023) The fragmentation-induced fluidisation of pyroclastic density currents. *Nat Commun* 14(1):2079. <https://doi.org/10.1038/s41467-023-37867-1>
- Brown RJ, Branney MJ (2013) Internal flow variations and diachronous sedimentation within extensive, sustained, density-stratified pyroclastic density currents flowing down gentle slopes, as revealed by the internal architectures of ignimbrites on Tenerife. *Bull Volcanol* 75(7):1–24. <https://doi.org/10.1007/s00445-013-0727-0>
- Brown RJ, Branney MJ, Maher C, Davila-Harris P (2010) Origin of accretionary lapilli within ground-hugging density currents: evidence from pyroclastic couplets on Tenerife. *Bull Geol Soc Am* 122(1–2):305–320. <https://doi.org/10.1130/B26449.1>
- Camuffo D (2019) Theoretical grounds for humidity. In: *Microclimate for Cultural Heritage*. Elsevier, pp 43–59. <https://doi.org/10.1016/B978-0-444-64106-9.00003-1>.
- Cas RA, Wright JV (1991) Subaqueous pyroclastic flows and ignimbrites: an assessment. *Bull Volcanol* 53(5):357–380. <https://doi.org/10.1007/BF00280227>
- Chédeville C, Roche O (2015) Influence of slope angle on pore pressure generation and kinematics of pyroclastic flows: insights from laboratory experiments. *Bull Volcanol* 77(11):96. <https://doi.org/10.1007/s00445-015-0981-4>
- Chédeville C, Roche O (2018) Auto fluidization of collapsing bed of fine particles: implications for the emplacement of pyroclastic flows. *J Volcanol Geotherm Res* 368:91–99. <https://doi.org/10.1016/j.jvolgeores.2018.11.007>
- Chen D, Zheng J, Zhang C, Guan D, Li Y, Yigang Wang (2021) Critical shear stress for erosion of sand-mud mixtures and pure mud. *Front Marine Sci* 8:713. <https://doi.org/10.3389/fmars.2021.713039>
- Chigira M, Yokoyama O (2005) Weathering profile of non-welded ignimbrite and the water infiltration behaviour within it in relation to the generation of shallow landslides. *Eng Geol* 78(3–4):187–207. <https://doi.org/10.1016/j.enggeo.2004.12.008>
- Cioni R, Pistolesi M, Rosi M (2015) Plinian and subplinian eruptions. In: *The encyclopedia of volcanoes*, 2nd edn. Academic Press, pp 519–535
- Cocco R, Reddy SB, Knowlton KT (2014) Back to basics introduction to fluidization. Available at: www.aiche.org/cep
- Cole PD, Calder ES, Druitt TH, Hoblitt R, Robertson R, Sparks RSJ, Young SR (1998) Pyroclastic flows generated by gravitational instability of the 1996–97 Lava Dome of Soufriere Hills Volcano, Montserrat. *Geophys Res Lett* 25(18):3425–3428. <https://doi.org/10.1029/98GL01510>
- Cole PD, Calder ES, Sparks RSJ, Clarke AB, Druitt TH, Young SR, Herd RA, Harford CL, Norton GE (2002) Deposits from dome-collapse and fountain-collapse pyroclastic flows at Soufriere Hills Volcano, Montserrat. *Geol Soc* 21:231–262
- Daag A, Westen CJ (1996) Cartographic modelling of erosion in pyroclastic flow deposits of Mount Pinatubo, Philippines. *ITC J* 2:110–124
- Dartevelle S, Ernst GGJ, Stix J, Bernard A (2002) Origin of the Mount Pinatubo climactic eruption cloud: implications for volcanic hazards and atmospheric impacts. *Geology* 7:663
- Deb PK, Abed SN, Jaber AMY, Tekade RK (2018) Particulate level properties and its implications on product performance and processing. *Dosage Form Design Parameters* 2:155–220. <https://doi.org/10.1016/b978-0-12-814421-3.00005-1>
- Dellino P, Dioguardi F, Isaia R, Sulpizio R, Male D (2021) The impact of pyroclastic density currents duration on humans: the case of the AD 79 eruption of Vesuvius. *Sci Rep* 11:4959. <https://doi.org/10.1038/s41598-021-84456-7>
- Douillet GA, Pacheco DA, Kueppers U, Letort J, Tsang-Hin-Sun E, Bustillos J, Hall M, Ramon P, Dingwell DB (2013) Dune bedforms produced by dilute pyroclastic density currents from the August 2006 eruption of Tungurahua volcano. *Ecuador Bull Volcanol* 75:762. <https://doi.org/10.1007/s00445-013-0762-x>
- Druitt TH (2014) New insights into the initiation and venting of the Bronze-Age eruption of Santorini (Greece), from component analysis. *Bull Volcanol* 76(2):794. <https://doi.org/10.1007/s00445-014-0794-x>
- Druitt TH, Bacon CR (1986) Lithic breccia and ignimbrite erupted during the collapse of Crater Lake Caldera, Oregon. *J Volcanol Geoth Res* 29(1–4):1–32. [https://doi.org/10.1016/0377-0273\(86\)90038-7](https://doi.org/10.1016/0377-0273(86)90038-7)

- Druitt TH, Bruni G, Lettieri P, Yates JG (2004) The fluidization behaviour of ignimbrite at high temperature and with mechanical agitation. *Geophys Res Lett* 31:L02604. <https://doi.org/10.1029/2003GL018593>
- Druitt TH, Avarid G, Bruni G, Lettieri P, Maez F (2007) Gas retention in fine-grained pyroclastic flow materials at high temperatures. *Bull Volcanol* 69:881–901. <https://doi.org/10.1007/s00445-007-0116-7>
- Duane WJ, Pepin NC, Losleben ML, Hardy DR (2008) General characteristics of temperature and humidity variability on Kilimanjaro, Tanzania. *Arct Antarct Alp Res* 40(2):323–334. <https://doi.org/10.1657/1523-0430>
- Dufek J (2016) The fluid mechanics of pyroclastic density currents. *Annu Rev Fluid Mech* 48:459–485. <https://doi.org/10.1146/annurev-fluid-122414-034252>
- Eychenne J, Pennec JLL, Troncoso L, Gouhier M, Nedelec JM (2012) Causes and consequences of bimodal grain-size distribution of tephra fall deposited during the August 2006 Tungurahua eruption (Ecuador). *Bull Volcanol* 74(1):187–205. <https://doi.org/10.1007/s00445-011-0517-5>
- Fisher RV, Schmincke HU (1984) Pyroclastic flow deposits. In: *Pyroclastic Rocks*. Springer Berlin, Heidelberg, pp 186–230. https://doi.org/10.1007/978-3-642-74864-6_8
- Geldart D (1973) Types of gas fluidization. *Powder Technol* 7:285–292. [https://doi.org/10.1016/0032-5910\(73\)80037-3](https://doi.org/10.1016/0032-5910(73)80037-3)
- Gilbertson MA, Taylor A, Mitchell S, Rust AC (2020) A fluidisation mechanism for secondary hydroeruptions in pyroclastic flow deposits. *Front Earth Sci* 8:324. <https://doi.org/10.3389/feart.2020.00324>
- Girolami L, Druitt T, Roche O, Khrabrykh ZV (2008) Propagation and hindered settling of laboratory ash flows. *J Geophys Res* B02202:113. <https://doi.org/10.1029/2007JB005074>
- Girolami L, Druitt TH, Roche O (2015) Towards a quantitative understanding of pyroclastic flows: effects of expansion on the dynamics of laboratory fluidized granular flows. *J Volcanol Geotherm Res* 296:31–39. <https://doi.org/10.1016/j.jvolgeores.2015.03.008>. (ISSN 0377-0273)
- Goel AP, Chopade SS (2020) Liquefied technology: preparation, characterization and applications. *J Drug Deliv Ther* 10(3-s):295–307. <https://doi.org/10.22270/jddt.v10i3-s.4067>
- Hall M, Mothes P, Ramon P, Arellano S, Barba D, Palacios P (2007) Dense pyroclastic flows of the 16–17 August 2006 eruption of Tungurahua Volcano, Ecuador. American Geophysical Union, Spring Meeting 2007, Abstract V33A-03
- Hartmann DL (2016) Global physical climatology, 2nd edn. In: *Vol 103 of International Geophysics*. Newnes
- Hausner HH (1981) Powder characteristics and their effect on powder processing. *Powder Technol* 30(1):3–8. [https://doi.org/10.1016/0032-5910\(81\)85021-8](https://doi.org/10.1016/0032-5910(81)85021-8)
- Houghton B, White JDL, Van Eaton AR (2015) Phreatomagmatic and related eruption styles. In: Sigurdsson H, Houghton B, Rymer H, Stix J, McNutt S (eds), *The Encyclopedia of Volcanoes*. Elsevier, pp 537–552. <https://doi.org/10.1016/B978-0-12-385938-9.00030-4>
- Huang Q, Zhang H, Zhu J (2009) Experimental study on fluidization of fine powders in rotating drums with various wall friction and baffled rotating drums. *Chem Eng Sci* 64(9):2234–2244. <https://doi.org/10.1016/j.ces.2009.01.047>
- Hurwitz S, Kipp KL, Ingebritsen SE, Reid ME (2003) Groundwater flow, heat transport, and water table position within volcanic edifices: implications for volcanic processes in the Cascade Range. *J Geophys Res* 108(B12). <https://doi.org/10.1029/2003JB002565>
- Keating GN (2005) The role of water in cooling ignimbrites. *J Volcanol Geotherm Res* 142(1–2 SPEC. ISS.):145–171. <https://doi.org/10.1016/j.jvolgeores.2004.10.019>
- Kelfoun K, Gueugneau V (2022) A unifying model for pyroclastic surge genesis and pyroclastic flow fluidization. *Geophys Res Lett* 49:e2021GL096517. <https://doi.org/10.1029/2021GL096517>
- Kelfoun K, Samaniego P, Palacios P, Barba D (2009) Testing the suitability of frictional behaviour for pyroclastic flow simulation by comparison with a well-constrained eruption at Tungurahua volcano (Ecuador). *Bull Volcanol* 71:1057–1075. <https://doi.org/10.1007/s00445-009-0286-6>
- Kim TH, Hwang C (2003) Modelling of tensile strength on moist granular earth material at low water content. *Eng Geol* 69(3–4):233–244. [https://doi.org/10.1016/s0013-7952\(02\)00284-3](https://doi.org/10.1016/s0013-7952(02)00284-3)
- Kim TH, Sture S (2008) Capillary-induced tensile strength in unsaturated sands. *Can Geotech J* 45(5):726–737. <https://doi.org/10.1139/T08-017>
- Lam D, Nakagawa M (1993) Packing of Particles (Part 2): Effect of extra pore volume on packing density of mixtures of monosized spheres. *J Ceram Soc Jpn* 101(11):1234–1238
- LaMarche CQ, Miller AW, Liu P, Hrenya C (2016) Linking micro-scale predictions of capillary forces to macro-scale fluidization experiments in humid environments. *AIChE J* 62(10):3585–3597. <https://doi.org/10.1002/aic.15281>
- Leturia M, Benali M, Lagarde S, Ronga I, Saleh K (2014) Characterization of flow properties of cohesive powders: a comparative study of traditional and new testing methods. *Powder Technol* 253:406–423. <https://doi.org/10.1016/j.powtec.2013.11.045>
- Li WC, Deng G, Liang XQ, Sun XX, Wang SW, Lee LM (2020) Effects of stress state and fine fraction on stress transmission in internally unstable granular mixtures investigated via discrete element method. *Powder Technol* 367:659–670. <https://doi.org/10.1016/j.powtec.2020.04.024>
- Lipman PW (2019) When ignimbrite meets water: mega scale gas-escape structures formed during welding. *Geology* 47(1):63–66. <https://doi.org/10.1130/G45772.1>
- Ludwig B, Millington-Smith D, Dattani R, Adair JH, Posatko EP, Mawby LM, Ward SK, Sills CA (2020) Evaluation of the hydrodynamic behaviour of powders of varying cohesivity in a fluidized bed using the FT4 Powder Rheometer®. *Powder Technol* 371:106–114. <https://doi.org/10.1016/j.powtec.2020.05.042>
- Ma Y, Evans TM, Phillips N, Cunningham N (2019) Modelling the effect of moisture on the flowability of a granular material. *Meccanica* 54(4–5):667–681. <https://doi.org/10.1007/s11012-018-0901-8>
- Manville V, Segschneider B, White JDL (2002) Hydrodynamic behaviour of Taupo 1800a pumice: implications for the sedimentology of remobilized pyroclasts. *Sedimentology* 49(5):955–976. <https://doi.org/10.1046/j.1365-3091.2002.00485.x>
- Matthews AJ, Barclay J, Johnstone JE (2009) The fast response of volcano-seismic activity to intense precipitation: triggering of primary volcanic activity by rainfall at Soufrière Hills Volcano, Montserrat. *J Volcanol Geoth Res* 184(3–4):405–415. <https://doi.org/10.1016/j.jvolgeores.2009.05.010>
- Montanari D, Agostini A, Bonini M, Corti G, Ventisette CD (2017) The use of empirical methods for testing granular materials in analogue modelling. *Materials* 10(6):635. <https://doi.org/10.3390/ma10060635>
- Moondra S, Maheshwari R, Tanja N, Tekade M, Tekadle RK (2018) Bulk level properties and its role in formulation development and processing. In: *Advances in Pharmaceutical Product Development and Research, Dosage Form Design Parameters*, vol 2. Academic Press, pp 221–256. <https://doi.org/10.1016/B978-0-12-814421-3.00006-3>
- Moyer TC, Swanson DA (1987) Secondary hydroeruptions in pyroclastic-flow deposits: examples from Mount St. Helens. *J Volcanol Geotherm Res* 32(4):299–319. [https://doi.org/10.1016/0377-0273\(87\)90081-3](https://doi.org/10.1016/0377-0273(87)90081-3)

- Pacheco-Hoyos JG, Aguirre-Díaz GJ, Dávila-Harris P (2020) Elutriation pipes in ignimbrites: an analysis of concepts based on the Huichapan Ignimbrite, Mexico. *J Volcanol Geotherm Res* 403:107026. <https://doi.org/10.1016/j.jvolgeores.2020.107026>
- Pensa A, Giordano G, Corrado S, Petrone PP (2023) A new hazard scenario at Vesuvius: deadly thermal impact of detached ash cloud surges in 79CE at Herculaneum. *Sci Rep* 13:5622. <https://doi.org/10.1038/s41598-023-32623-3>
- Pepin NC, Pike G, Schaefer M, Boston CM, Lovell H (2017) A comparison of simultaneous temperature and humidity observations from the SW and NE slopes of Kilimanjaro: the role of slope aspect and differential land-cover in controlling mountain climate. *Global Planet Change* 157:244–258. <https://doi.org/10.1016/j.gloplacha.2017.08.006>
- Pierrat P, Caram HS (1997) Tensile strength of wet granula materials. *Powder Technol* 97(2):83–93. [https://doi.org/10.1016/S0032-5910\(96\)03179-8](https://doi.org/10.1016/S0032-5910(96)03179-8)
- Riehle JR, Miller TF, Bailey RA (1995) Cooling, degassing and compaction of rhyolitic ash flow tuffs: a computational model. *Bull Volcanol* 57:319–336. <https://doi.org/10.1007/BF00301291>
- Rios M (2006) Developments in powder flow testing. *Pharm Technol* 30(2):38–49
- Roche O (2012) Depositional processes and gas pore pressure in pyroclastic flows: an experimental perspective. *Bull Volcanol* 74:1807–1820. <https://doi.org/10.1007/s00445-012-0639-4>
- Roche O, Druitt TH, Cas RAF (2001) Experimental aqueous fluidization of ignimbrite. *J Volcanol Geotherm Res* 112(1–4):267–280. [https://doi.org/10.1016/S0377-0273\(01\)00246-3](https://doi.org/10.1016/S0377-0273(01)00246-3)
- Roche O, Gilbertson MA, Phillips JC, Sparks RS (2004) Experimental study of gas-fluidized granular flows with implications for pyroclastic flow emplacement. *J Geophys Res Solid Earth* 109:B10201. <https://doi.org/10.1029/2003JB002916>
- Sahoo S, Tiwari DK, Panda D, Kundu B (2022) Eruption cycles of Mount Etna triggered by seasonal climatic rainfall. *J Geodyn* 149. <https://doi.org/10.1016/j.jog.2021.101896>
- Schneider CA, Rasband WS, Eliceiri KW (2012) NIH Image to ImageJ: 25 years of image analysis. *Nat Methods* 9:671–675
- Self S, Sparks RSJ (1978) Characteristics of widespread formed by the interaction of silicic magma and water pyroclastic deposits. *Bull Volcanol* 41:196–212
- Shimizu HA, Koyaguchi T, Suzuki YJ (2023) Dynamics and deposits of pyroclastic density currents in magmatic and phreatomagmatic eruptions revealed by a two-layer depth-averaged model. *Geophysical Research Letters* 50(16):616. <https://doi.org/10.1029/2023GL104616>
- Smith GM (2020) Propagation of aerated pyroclastic density current analogues: flow behaviour and the formation of bedforms and deposits. Dissertation, University of Hull
- Sparks RSJ (1976) Grain size variations in ignimbrites and implications for the transport of pyroclastic flows. *Sedimentology* 23(2):147–188. <https://doi.org/10.1111/j.1365-3091.1976.tb00045.x>
- Sparks RSJ (1978) Gas release rates from pyroclastic flows: a assessment of the role of fluidisation in their emplacement. *Bull Volcanol* 41(1):1–9. <https://doi.org/10.1007/BF02597679>
- Telling J, Dufek J, Shaikh A (2013) Ash aggregation in explosive volcanic eruptions. *Geophys Res Lett* 40(10):2355–2360. <https://doi.org/10.1002/grl.50376>
- The United States Pharmacopeial Convention (2015) Bulk density and tapped density of powders - US pharmacopeia (USP), (616) Bulk Density and Tapped Density of Powders. Available at: https://www.usp.org/sites/default/files/usp/document/harmonization/genchapter/bulk_density.pdf (Accessed: 02 June 2023).
- Valentine G, Sweeney M (2018) Compressible flow phenomena at inception of lateral density currents fed by collapsing gas-particle mixtures. *J Geophys Res: Solid Earth* 123(2):1286–1302. <https://doi.org/10.1002/2017JB015129>
- Van Eaton AR, Wilson CJN (2013) The nature, origins and distribution of ash aggregates in a large-scale wet eruption deposit: Oruanui, New Zealand. *J Volcanol Geoth Res* 250:129–154. <https://doi.org/10.1016/j.jvolgeores.2012.10.016>
- van Westen CJ, Daag AS (2005) Analysing the relation between rainfall characteristics and lahar activity at Mount Pinatubo, Philippines. *Earth Surf Process Landf* 30(13):1663–1674. <https://doi.org/10.1002/esp.1225>
- Vecino MCD, Rossi E, Freret-Logeril V, Fries A, Gabellini P, Lemus J, Pollastri S, Poulidis AP, Iguchi M and Bonadonna C (2022) Aerodynamic characteristics and genesis of aggregates at Sakurajima Volcano, Japan. *Sci Rep* 14. <https://doi.org/10.1038/s41598-022-05854-z>
- Wilson CJN (1980) The role of fluidization in the emplacement of pyroclastic clasts: an experimental approach. *J Volcanol Geotherm Res* 8(2–4):231–249. [https://doi.org/10.1016/0377-0273\(80\)90106-7](https://doi.org/10.1016/0377-0273(80)90106-7)
- Wilson CJN (1984) The role of fluidization in the emplacement of pyroclastic flows, 2: experimental results and their interpretation. *J Volcanol Geoth Res* 20(1–2):55–84. [https://doi.org/10.1016/0377-0273\(84\)90066-0](https://doi.org/10.1016/0377-0273(84)90066-0)
- Wormsbecker M, Pugsley T (2008) The influence of moisture on the fluidization behaviour of porous pharmaceutical granule. *Chem Eng Sci* 63(16):4063–4069. <https://doi.org/10.1016/j.ces.2008.05.023>
- Yehuda T, Kalman H (2020) Geldart classification for wet particles. *Powder Technol* 362:288–300. <https://doi.org/10.1016/j.powtec.2019.11.073>
- Yu AB, Hall JS (1994) Packing of fine powders subjected to tapping. *Powder Technol* 78(3):247–256. [https://doi.org/10.1016/0032-5910\(93\)02790-H](https://doi.org/10.1016/0032-5910(93)02790-H)